



## Modeling, simulation and PI gain-scheduling controller optimization of water desalination plant with liquid jet vacuum ejector

Miloš Lomović<sup>a,\*</sup>, Andrija A. Petrović<sup>b</sup>, Milan Ristanović<sup>a</sup>, Aleksandar Petrović<sup>b</sup>

<sup>a</sup>Department of Automatic Control, University of Belgrade Faculty of Mechanical Engineering, Kraljice Marije 16, 11000 Belgrade, Serbia, Tel. +381 63 280 270; email: mlomovic@gmail.com (M. Lomovic), Tel. +381 63 81 41 397; email: mristanovic@mas.bg.ac.rs (M. Ristanovic)

<sup>b</sup>Department of Process Engineering, University of Belgrade Faculty of Mechanical Engineering, Kraljice Marije 16, 11000 Belgrade, Serbia, Tel. +381 62 295 278; emails: aapetrovic@mas.bg.ac.rs (A.A. Petrovic), apetrovic@mas.bg.ac.rs (A. Petrovic)

Received 17 March 2018; Accepted 28 September 2018

---

### ABSTRACT

This paper gives a novel approach to modeling, simulation and control of a water desalination plant. The process in desalination plant is based on a vapour compression acquired by a liquid jet vacuum ejector. Optimal plant design for a nominal operating point is obtained using the combination of the multi-objective optimization with the multi-criteria decision making. Furthermore, the dynamic steady-state model which includes a liquid jet vacuum ejector, pump, valve and pressure vessel is developed. Moreover, for the different values of inlet temperature and water mass flow rate (disturbances) the optimal regimes of system actuators are found by the antlion algorithm, with respect to the profit maximization. Also, the control-oriented model of the system has been developed and linearized around different operating points to design a gain-scheduling nonlinear proportional integral controller. Additionally, it is demonstrated that the proposed controller is capable of guiding the system through the optimal states under the influence of disturbances. A map of the controller gains is determined by extensive simulation minimizing the appropriate cost functions. High-fidelity model has been numerically simulated in order to demonstrate that the developed method provides the desired design specifications while minimizing operational costs.

*Keywords:* Multi-objective optimization; Desalination; Process modeling; Process control; Gain-scheduling nonlinear PI control

---

### 1. Introduction

It is widely known that there is a limited amount of drinking water on the earth. Unfortunately, this water is not distributed evenly throughout the planet. The increasing demand for desalinated water, caused by the rapid growth of industries in the underdeveloped areas of the world, imposes the need for improvements in the production process of desalinated water with lower costs [1,2]. Current trends in technology development and cost reduction are based on methods such as multi-stage flash distillation (MSF), multi-effect distillation (MED), vapour compression (VC), reverse osmosis (RO) and electrodialysis. It is expected

that MSF, MED and RO will be the most dominant methods in the future [3,4].

Thermal and electrical energies are necessary for a wide variety of approaches, whereas RO consumes only electrical energy. Furthermore, one of the benefits of RO methods is an energy recovery system, which makes them the most cost-effective methods. Different studies are dealing both with the dynamic and steady-state models of RO plants [5,6]. Moreover, there is a huge number of advanced techniques for dynamical modeling [7,8]. Presented dynamic models were used for simulation and control system designs as shown in the studies by Phuc et al. [9], Assef et al. [10] and Bartman et al. [11].

---

\* Corresponding author.

Regarding thermal procedures for water desalination, current interest is on using renewable energy sources. Special trends are based on the utilization of solar energy for process heating [12]. A lot has been done in the field of modeling, simulation and optimization of solar evaporation systems for desalination [13–15].

RO has been the most utilized method for desalination because it has several advantages over other methods. However, when it comes to the process of desalination from geothermal water, the VC method presented in this paper has shown good results. Utilization of geothermal energy for water desalination can be achieved in two ways: by direct evaporation of hot water, which emerges on the surface (geysers and hot springs), or indirectly, using geothermal energy for heating and evaporating water [16,17]. Significant improvements in the technology of water desalination from geothermal sources have not been observed in the last period, so more and more attention is paid to the optimization of thermodynamic parameters of the existing cycle to obtain lower investment, operational costs and less impact on the environment [18].

This paper has a goal to show a novel approach of modeling, simulation and control of the water desalination plant based on VC with a liquid jet vacuum ejector. The system description and problem statement are presented in Section 2.

Plant design for nominal operating point was carried out by the multi-objective optimization (MOP) with the multi-criteria decision-making (MCDM) method, as presented in Section 3. Due to monthly changes of inlet water temperature and flow rate, it was necessary to acquire optimal working regimes for system actuators (pumps and valves) with respect to profit maximization for different operating points.

In Section 4, nonlinear dynamical model for control purposes is derived and verified by applying the results of the

steady-state simulation. Bearing in mind slow changes in the disturbances, controls strategy is studied. Furthermore, the model is linearized and validated using the previously obtained nonlinear model and two control gain-scheduling algorithms, linear and nonlinear. The proposed algorithms have the goal to guide the plant through optimal states for different operating points.

Results of numerical simulation are presented in Section 5. The worst case scenario is applied in order to test the control algorithms. Additionally, a family of proportional integral (PI) controllers are chosen, tuned and compared. Finally, conclusion and key findings are given in Section 6.

## 2. System description and problem statement

### 2.1. System description

The water desalination plant under consideration is shown in Fig. 1. It is supplied with a geothermal water from one or more hot springs through the balancing tank for desalination (BTD). By maintaining a constant level in the BTD, a constant flow through the valve V1 into the vessel P1 is ensured. The vessel P1 is under pressure lower than the pressure corresponding to the evaporation temperature of the inlet water. Low pressure in the vessel P1 is maintained using the liquid jet vacuum ejector E1. A saturated steam is entrained in the ejector E1. Due to the low entrained ratio (ER) the steam is completely condensed in the ejector. Therefore, to hold the constant water temperature ( $t_{104}$ ) at the steady-state regime a heat exchanger HE1 is utilized. The inlet and the outlet temperatures of the cold fluid (river water) in HE1 are assumed to be equal and constant. The purpose of pump PU2 is to drain boiled water and to maintain a constant liquid

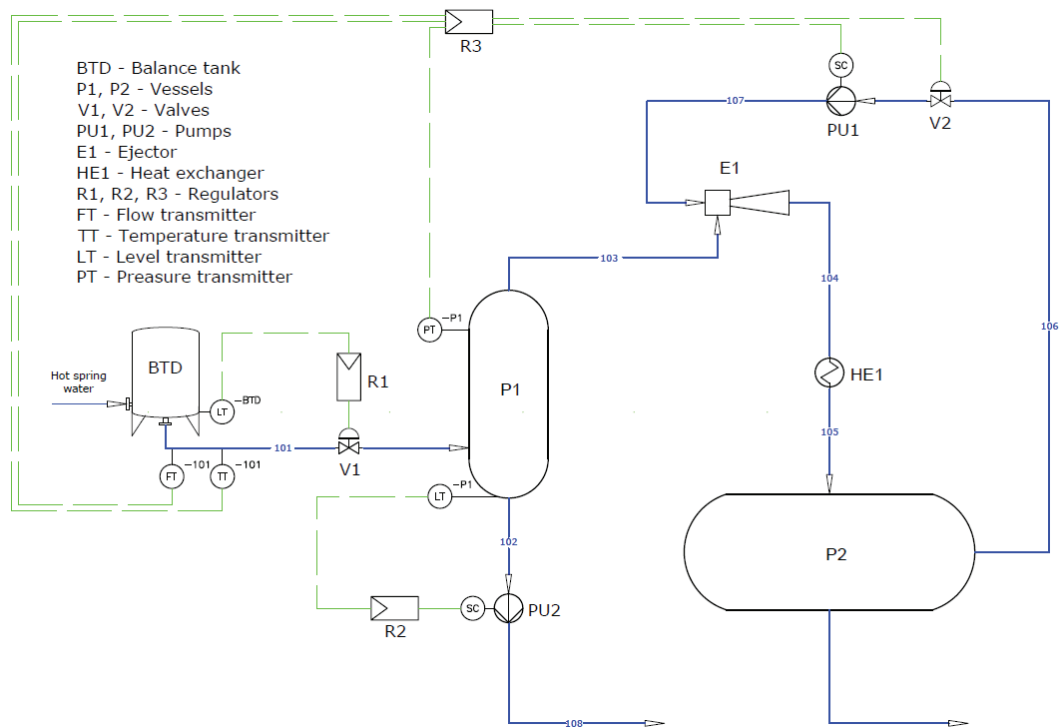


Fig. 1. PID and control structure of a water desalination plant.

level in the vessel P1. Pump PU1 together with valve V2 control the pressure in the vessel P1 indirectly. Vessel P2 is used to supply a part of the desalinated water to the consumers and maintain a constant level of water necessary for the normal operation of the pump PU1.

Pumps PU1 and PU2 are controlled by frequency converters, while V1 and V2 are control valves. Level transmitters (LT)-BTD and LT-P1 have been mounted at the BTD and P1, respectively. Similarly the pressure transmitter measures pressure in the P1.

## 2.2. Problem statement

The plant design has been done for nominal operating points ( $\dot{m}_{101} = 1.0 \text{ kg/s}$  and  $t_{101} = 82^\circ\text{C}$ ) with respect to minimization of exergy loss, investment costs and profit maximization.

Due to monthly changes, the temperature and mass flow rates of geothermal mineral water are varying. During the winter, the temperature of the geothermal water is decreasing to  $65^\circ\text{C}$ , while in the summer the temperature can increase up to  $82^\circ\text{C}$ . Analogously, the mass flow rates vary as well. During the summer the mass flow rates can decrease to  $0.05 \text{ kg/s}$ . On the other hand, during the winter it can have a value up to  $1 \text{ kg/s}$  (Fig. 2). Therefore, these parameters are modeled as disturbances.

The constant water levels in the BTD and P1 are controlled by controllers R1 and R2 (Fig. 1) by means of valves V1 and V2, respectively.

Commonly the pump for the motive fluid does not have a controller, thus, it operates at a fixed frequency which is

provided by the power network (50 or 60 Hz). Therefore, one of the disadvantages is the possibility of the ejector cavitation that could occur when the disturbance takes place. In addition, there is no guarantee that the system shall have the maximum effectiveness of its capacity for different values of inlet mass flow rates and temperatures (State 101). To avoid mentioned problems, in order to maximize the capacity and, therefore, the profit, it is necessary to determine the optimal operating point for different values of inlet temperature ( $t_{101}$ ) and mass flow rate ( $\dot{m}_{101}$ ) applying a single-objective optimization.

The optimal operating points can be achieved by introducing the controller R3, whose purpose is to control the system through the optimal trajectory under the influence of disturbances. Controller R3 leads the pump's PU1 frequency and at the same time the hydraulic resistance of the valve V1. The inlet temperature ( $t_{101}$ ) and mass flow rate ( $\dot{m}_{101}$ ) are measured disturbances, whereas pressure  $p_{102}$  is the manipulated variable of the controller R3.

In order to simplify the problem, certain reasonable assumptions have been introduced. Because the tuning of controllers R1 and R2 is a trivial control problem, it is assumed that both of them are perfectly tuned, working within the desired limits. Thus, the water levels in BTD and P1 are constant. In addition, heat loss in the vessel P2 is negligible, so  $t_{104} = t_{106}$ . Following the assumptions, the system diagram can be simplified (Fig. 3).

## 3. Optimization: modeling and simulation

In this section, steady-state modeling and plant design are conducted using MOP along with MCDM.

Firstly, the core theory used in this chapter is presented in Subsection 3.1. Then, the design of the water desalination plant was carried out by the MOP in Subsection 3.2, followed by steady-state simulation and optimization of the plant operation in Subsection 3.3. At the end of the section, the optimization results are presented in Subsection 3.4.

### 3.1. Theoretical background

#### 3.1.1. MOP—non-dominated sorting genetic algorithm (NSGA-II) method

MOP has been defined as a finding vector of decision variables satisfying constraints to give acceptable values to all objective function. Mathematically defined MOP can be expressed as follows: find the vector  $X^* = [x_1^*, x_2^*, \dots, x_n^*]$  to optimize  $F(X) = [f_1^*(x), f_2^*(x), \dots, f_n^*(x)]$ , subject to  $m$  inequality constraints  $g_i(X) \leq 0$  and  $p$  equality constraint  $h_j(X) = 0$ .

Without loss of generality, it can be assumed that all of the objective function has to be minimized. In general, objective functions are not in consistency, such that minimization of one objective does not lead to a minimization of the others. Because of that goal of the MOP is based on finding Pareto optimal decision vectors (Pareto set)  $P^* = \{X \in \Omega \mid \nexists X' \in \Omega: F(X') < F(X)\}$  along with the Pareto front  $PF^* = \{F(X) = (f_1(x), f_2(x), \dots, f_n(x))\}$ . More definitions concerning Pareto optimality, Pareto dominance, etc. can be found in the study by Coello [19].

In this paper, we use NSGA-II proposed by Deb et al. [20]. NSGA-II is the type of evolutionary algorithm commonly

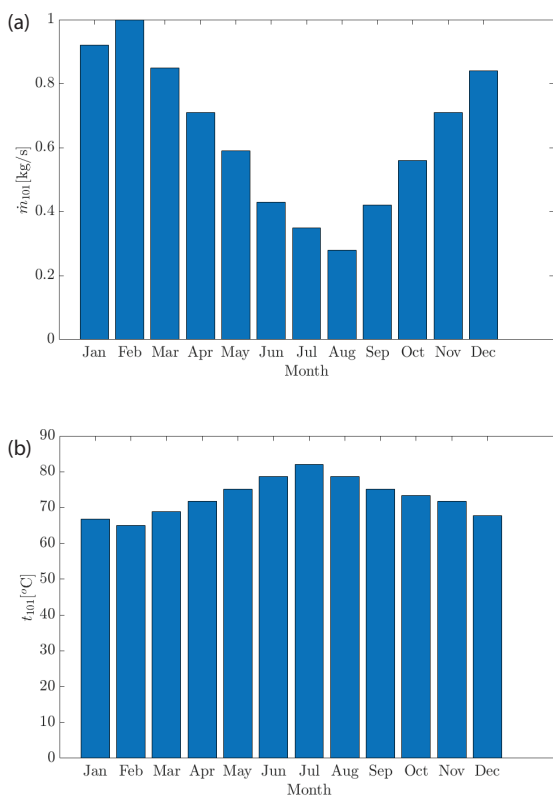


Fig. 2. Changes of (a)  $\dot{m}_{101}$  and  $t_{101}$  during a year.

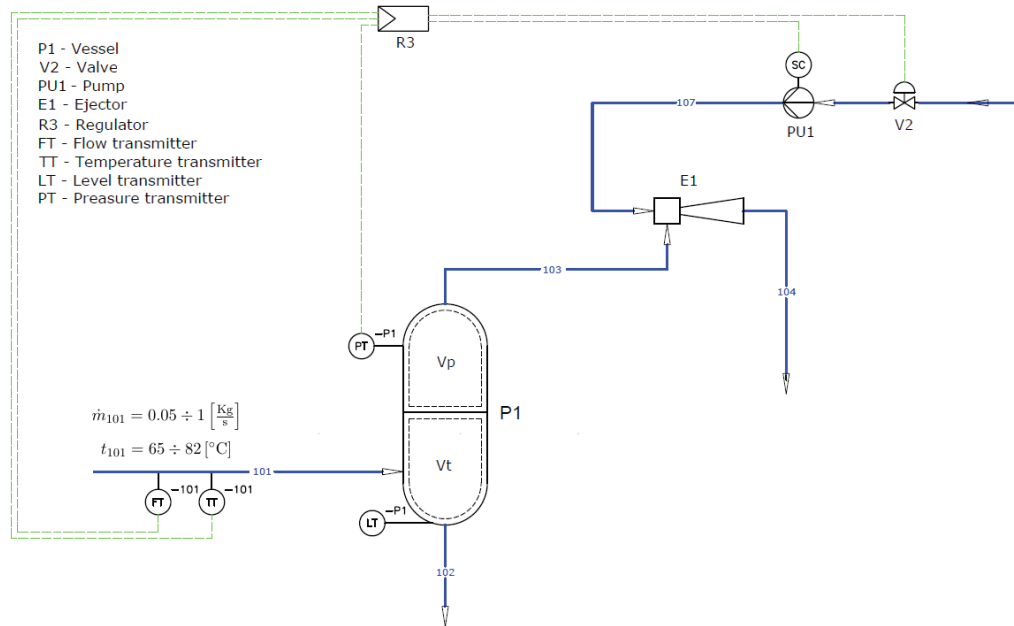


Fig. 3. PID and control structure of a simplified water desalination plant.

used for MOP problems. It is a modified version of original NSGA and has a better sorting algorithm, incorporates elitism and has no sharing parameter needs to be chosen a priori.

The pseudo code of algorithm [21] is presented as Algorithm 1.

### 3.1.2. Analytic hierarchy process (AHP)–simple additive weighting (SAW) method

One class of approaches for solving MCDM problems are based on the well-known AHP, which reduces complex decisions to a series of pairwise comparisons and synthesizes the results [22].

AHP enables comparison of alternatives, by a specific criterion, in pairs, on the basis of which the assessment matrix is formed. Sati’s scale gives a sufficiently precise comparison. In this scale, the criteria are compared with numbers 1 to 9. Preference matrix is expressed as follows:

$$MP = \begin{pmatrix} 1 & \dots & X_{1n} \\ \vdots & \ddots & \vdots \\ X_{1n} & \dots & 1 \end{pmatrix} \quad (1)$$

The decision-makers consistency is measured by a consistency ratio calculated as follows:

$$CR = \frac{\lambda_{\max} - n}{(n-1)RI} \quad (2)$$

where  $\lambda_{\max}$  is the highest eigenvalue of the assessment matrix;  $n$  is the number of alternatives and RI is a coefficient that depends on the number of alternatives to be compared.

SAW which is also known as a weighted linear combination or scoring methods is one of the simplest and most

### Algorithm 1. NSGA-II algorithm

```

begin
generate P0 at random
set P0 = (F1, F2, ...) = non-dominated-sort(P0)
for all Fi ∈ P0 do
    crowding-distance-assignment(Fi)
end for
set t = 0
while not done do
    generate child population Qt from Pt
    set Rt = Pt ∪ Qt
    set F = (F1, F2, ...) = non-dominated-sort(Rt)
    set Pt+1 = ∅
    set i = 1
    while |Pt+1| + |F| < N do
        crowding-distance-assignment(Fi)
        set Pt+1 = Pt+1 ∪ Fi
        set i = i + 1
    end while
    sort Fi on crowding distances
    set Pt+1 = Pt+1 ∪ Fi[1: (N - |Pt+1|)]
    set t = t + 1
end while
return F1
end
    
```

often used in combination with AHP. The additional details of AHP–SAW methodology are presented in [23].

### 3.1.3. The antlion optimizer

The antlion optimizer (ALO) is a type of metaheuristic algorithm used for single-objective optimizations, which was first introduced by Mirjalili [24]. The ALO mimics the interaction between antlions and ants in the trap, such that ants are moving over the search spaces, whereas antlions are hunting

them and becoming fitter using traps. The movement of ants is purely stochastic, and random walk is chosen as a model of ants movements. Beside ants, antlions are also hiding in search space. Similarly, positions and fitness functions of the ants are also stored in matrices. Ants update random walk in every iteration, and a random walk is normalized in order to keep it in search space (Eq. (3)). After each iteration, ants and antlions positions along with the evaluated fitness functions are stored in matrices. It should be noted that the random walk of ants is affected by antlion traps presented in Eqs. (4) and (5).

$$X_i^t = \frac{(X_i^t - a_i)(d_i^t - c_i^t)}{(b_i - a_i)} + c_i \quad (3)$$

$$c_i^t = \text{Antlion}_j^t + c^t \quad (4)$$

$$d_i^t = \text{Antlion}_j^t + d^t \quad (5)$$

where  $a_i$  is the minimum of random walk of  $i$ -th variable,  $b_i$  is maximum of random walk of  $i$ -th variable,  $c_i^t$  is minimum of  $i$ -th variable at  $t$ -th iteration,  $d_i^t$  is maximum of  $i$ -th variable at  $t$ -th iteration,  $c^t$  is the minimum of all variables at  $t$ -th iteration and  $d^t$  is the maximum of all variables at  $t$ -th iteration.

The radius of ants random walk hypersphere is decreased with each iteration (Eqs. (6) and (7)).

$$c^t = \frac{\text{lb}}{I} \quad (6)$$

$$d^t = \frac{\text{ub}}{I} \quad (7)$$

where lb is lower bound of search space, ub is upper bound of search space and  $I$  is iteration coefficient.

Positions of the antlions are influenced by the position of the fittest ants. Furthermore, an antlion updates its position to the position of the ant if the following requirement is satisfied:

$$f(\text{Ant}_i^t) > f(\text{Antlion}_j^t) \rightarrow \text{Antlion}_j^t = \text{Ant}_i^t \quad (8)$$

where  $t$  shows the current iteration,  $\text{Ant}_i^t$  indicates position of the  $i$ -th ant at  $t$ -th iteration and  $\text{Antlion}_j^t$  is position of  $j$ -th antlion at  $t$ -th iteration.

Elitism in ALO is introduced by choosing the fittest antlion. Besides, it is assumed that every ant randomly walks around a selected antlion and elite as follows:

$$\text{Ant}_i^t = \frac{R_A^t + R_E^t}{2} \quad (9)$$

where  $R_A^t$  is a random walk around the antlion selected by the roulette wheel at  $t$ -th iteration and  $R_E^t$  is the random walk around the elite at the  $t$ -th iteration.

Pseudocode of the ALO is presented in Algorithm 2, and additional explanation of the ALO can be seen in the study by Mirjalili [24].

### 3.2. Mathematical modeling

In this study, the design of the water desalination plant was carried out by the MOP. NSGA-II algorithm did not show satisfactory performances in three objective optimizations, hence, two-objective optimization has been considered.

Water desalination plant along with all thermodynamic states of process fluids is presented in Fig. 3. The goal of MOP and MCDM is to minimize the total investment costs ( $C_{\text{inv}}$ ) and exergy loss (EXloss) while maximizing profit. The total exergy loss is added as additional discrete criteria in MCDM, whereas  $C_{\text{inv}}$  and profit were used as objective functions in MOP. The MOP is performed by varying the following thermophysical properties  $q = \dot{V}_{107} / \dot{V}_{103}$ ,  $p_{102}$  and  $t_{104}$ . Thermodynamic states of the plant can be determined by the mass and energy balances. The constant values of the thermodynamic states are presented in Table 1. The following assumptions have been introduced:

1. The friction losses in heat exchanger, pipes and pressure vessels are neglected;
2. Water is assumed to be pure  $\text{H}_2\text{O}$ ;
3. Environmental conditions of the ambient temperature and pressure are also used for enthalpy and exergy calculations;

Algorithm 2. The antlion optimizer algorithm

```

begin
Initialize the first population of ants and antlions randomly
Calculate the fitness of ants and antlions
Find the best antlions and assume it as the elite (determined optimum)
while the end criterion is not satisfied do
  for all every ant do
    Select an antlion using Roulette wheel
    Update  $c$  and  $d$  using Eqs. (4) and (5)
    Create a random walk and normalize it using Eq. (3)
    Update the position of ant using Eq. (9)
  end for
  Calculate fitness of all ants
  Replace an antlion with its corresponding ant if it becomes fitter using Eq. (8)
  Update elite if an antlion becomes fitter
end while
return elite
end

```

Table 1  
Constant thermophysical states of water desalination plant

$t_{\text{river}}$ K	293.15
$t_{\text{amb}}$ K	293.15
$\dot{m}_{101}$ kg/s	1
$p_{101}$ Pa	101,325
$p_{104}$ Pa	101,235
$p_{105}$ Pa	101,325
$p_{108}$ Pa	101,325
$t_{101}$ K	355.15
$p_{\text{amb}}$ Pa	101,235

4. Heat loss in surrounding is neglected;
5. Averaged fluids thermophysical characteristics are used in heat exchanger calculations; and
6. Constant total heat transfer coefficient in HE1 is  $k = 1,000 \text{ W/m}^2\text{K}$ .

The thermophysical properties and thermodynamic states are calculated by CoolProp [25].

Applying the experimental equations given in the study by Sokolov [26], the inlet motive fluid mass flow rate, pressure and exergy loss are found by Eqs. (10)–(12), respectively.

$$\dot{m}_{107} = \frac{\dot{m}_{103} \cdot 15}{\rho_{103} \cdot q} \cdot \rho_{107} \quad (10)$$

$$p_{107} = (p_{104} - p_{103}) \cdot 1.4 \cdot \left(1 + \frac{q}{15}\right)^2 + p_{103} \quad (11)$$

$$\text{EXloss}_{E1} = t_{\text{amb}} \cdot (\dot{m}_{102} s_{102} + \dot{m}_{103} s_{103} - \dot{m}_{101} s_{101}) \quad (12)$$

Energy and exergy balance of the heat exchanger HE1 are shown in Eqs. (13) and (14), whereas the total surface area of HE1 is calculated by Eq. (15).

$$Q_{\text{HE1}} = \dot{m}_{104} h_{104} - \dot{m}_{105} h_{105} \quad (13)$$

$$\text{EXloss}_{\text{HE1}} = t_{\text{amb}} \cdot \left( \dot{m}_{105} s_{105} - \dot{m}_{104} s_{104} + \frac{Q_{\text{HE1}}}{t_{\text{amb}}} \right) \quad (14)$$

$$S_{\text{HE1}} = \frac{Q_{\text{HE1}}}{k_{\text{HE1}} \cdot \Delta t_{\text{mean,HE1}}} \quad (15)$$

Energy and exergy balances for the vessel P1 are as follows:

$$\dot{m}_{101} h_{101} = \dot{m}_{102} h_{102} + \dot{m}_{103} h_{103} \quad (16)$$

$$\text{EXloss}_{P1} = t_{\text{amb}} \cdot (\dot{m}_{102} s_{102} + \dot{m}_{103} s_{103} - \dot{m}_{101} s_{101}) \quad (17)$$

The energy and exergy balances of the PU1 and PU2 can be determined, in the same manner, as follows:

$$h_{\text{out}} = \frac{h_{\text{out,ideal}} - h_{\text{in}}}{\eta_{\text{adb}}} + h_{\text{in}} \quad (18)$$

$$P_{\text{PU}^*} = h_{\text{out}} - h_{\text{in}} \quad (19)$$

$$\text{EXloss}_{\text{PU}^*} = t_{\text{amb}} \cdot (\dot{m}_{\text{out}} s_{\text{out}} - \dot{m}_{\text{in}} s_{\text{in}}) \quad (20)$$

Total exergy loss of the water desalination plant is as follows:

$$\text{EXloss}_{\text{tot}} = \text{EXloss}_{\text{HE1}} + \text{EXloss}_{E1} + \text{EXloss}_{\text{PU1}} + \text{EXloss}_{\text{PU2}} + \text{EXloss}_{P1} \quad (21)$$

Daily profit of water desalination plant is calculated by subtracting costs of electricity (it is assumed that other costs are negligible) from plant revenue:

$$\text{Profit} = 24 \cdot \left( \dot{m}_{103} \cdot 3600 \cdot \text{price}_{\text{water}} - \frac{(P_{\text{PU1}} + P_{\text{PU2}})}{1000} \cdot \text{costs}_{\text{ei}} \right) \quad (22)$$

where  $\text{price}_{\text{water}}$  is the water price per 1 kg of the water and  $\text{costs}_{\text{ei}}$  is the electricity costs per 1 kWh of the electrical energy.

Total investment costs are calculated by detail factor analysis method [27] as follows:

$$C_{\text{INV}} = C_{\text{ISBL}} \cdot (f_{\text{ISBL}} + f_{\text{ISBL}} f_{\text{OSBL}}) \cdot (1 + f_{\text{ENG}} + f_{\text{CONT}}) \quad (23)$$

$$f_{\text{ISBL}} = 1 + f_1 + f_2 + f_3 + f_4 + f_5 + f_6 + f_7 \quad (24)$$

where  $C_{\text{ISBL}}$  is a total cost of equipment;  $C_{\text{ISBL}}$  is expressed for every piece of the equipment as shown in Table 2.

Values of coefficients in Eqs. (23) and (24) are shown in Table 3. Additionally, different authors expressed cost functions for a different time period, because of that functions are modified by Chemical Engineering Plant Cost Index (CEPCI) for 2013. More details about CEPCI influential factors can be observed in the study by Vatavuk et al. [29]

In order to get reasonable results from MOP, following constraints are added:

$$m_i > 0 \quad (25)$$

$$\Delta t_{\text{mean,HE1}} > 0 \quad (26)$$

$$\Delta t_{\text{mean,HE1}} \in \mathcal{R} \quad (27)$$

The Pareto front, with 100 optimal alternatives obtained by performing NSGA-II algorithm, is shown in Fig. 4(a),

Table 2

The cost functions of various equipments in the water desalination plant [27,28]

System component	Cost functions
Pump	$C_{\text{ISBL,PU}} = (3300 + 48 \cdot \dot{V}^{1.2}) \cdot \frac{925.8}{478.6}$
Ejector	$C_{\text{ISBL,E}} = 148.4 + 18.04 \cdot D_{\text{diffuser}} - 002752 \cdot D_{\text{diffuser}}^2$
Heat exchanger	$C_{\text{ISBL,HE}} = (6460 + 64.5 \cdot S_{\text{HE}}^{0.97}) \cdot \frac{621.6}{394}$
Vessel	$C_{\text{ISBL,P}} = 780 \cdot V^{0.72} \cdot \frac{567.5}{478.6}$

while in Fig. 4(b) the whole space of decision alternatives is presented.

From the obtained Pareto front, the investor should decide which plant to choose. Therefore, the investor must show his/her preferences according to the given criteria. Bearing in mind that the investment cost is still the most important

Table 3  
Values of coefficients used in the evaluation of total investment costs

Position	Label	Value
Installation of equipment	$f_1$	0.2
Pipes, ducts, etc.	$f_2$	0.2
Measuring and automation equipment	$f_3$	0.3
Electrical equipment and work	$f_4$	0.2
Construction works	$f_5$	0.05
Load-bearing structures and buildings	$f_6$	0.05
Protective works	$f_7$	0.05
ISBL factor	$f_{ISBL}$	2.05
OSBL factor	$f_{OSBL}$	0.1
Engineering	$f_{ENG}$	0.3
Unexpected expenses	$f_{CONT}$	0.1

ISBL — Inside battery limits; OSBL — outside battery limits.

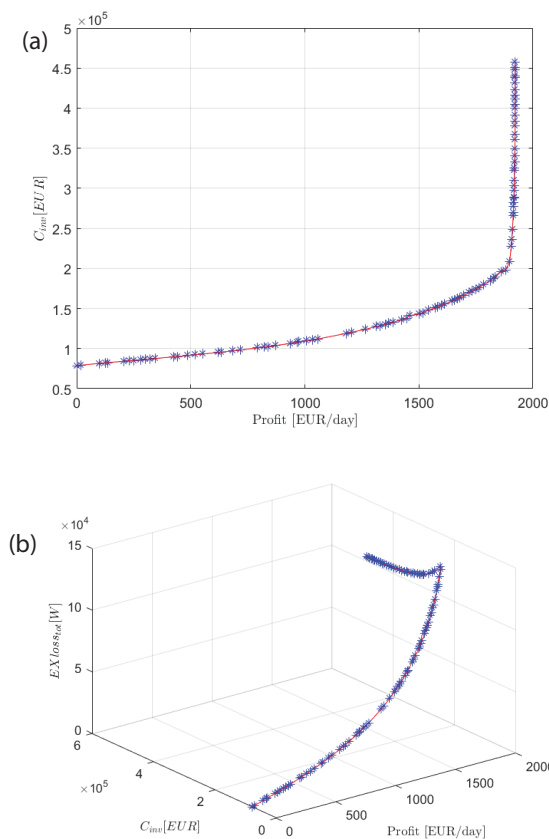


Fig. 4. (a) Pareto front of optimal decision and (b) MCDM alternatives.

motive of the investor, it follows that the maximization of the profit is the crucial factor, whereas the least significant criterion is the sustainability of the plant. The AHP preference matrix for the three criteria, set in the order of profit, investment, exergy loss, is given by the Eq. (28).

$$MP = \begin{bmatrix} & \text{Profit} & \text{Investment} & \text{Exergy loss} \\ \text{Profit} & 1 & 3 & 9 \\ \text{Investment} & 0.333 & 1 & 3 \\ \text{Exergy loss} & 0.111 & 0.333 & 1 \end{bmatrix} \quad (28)$$

The optimal alternative 65 (Fig. 5) is made such that consistency ratio is  $CR = 0$ . The weight factors determined by the AHP method is  $w = [0.69 \ 0.23 \ 0.078]$ .

The alternatives of the plant are sorted in the direction of growth of profit increase; so the sensitivity analysis can show that the change in the weight, (or preferences) of the decision maker, influences the change in the choice of the alternative. The sensitivity analysis is shown in Fig. 12.

Based on the sensitivity analysis, it can be observed that for values of the high-profit weights, the optimal decision tends to the alternatives with the highest profit and investment cost. Whereas the higher weights values of the investments and exergy losses lead to the alternatives where production of the desalinated water is low. It is also noteworthy that the alternative 65 is robust, that is, in a wide range of movements, the weight of profit, investment and exergy losses does not change. In accordance with the alternative 65, following geometric dimensions of the plant are obtained and presented in Table 4.

### 3.3. Steady-state simulation and optimization of plant operation

After evaluating the results of the combination of MOP and MCDM, the optimal plant design in the nominal operating point is selected.

Due to the change of seasons, the temperature and mass flow rates of mineral water are varying. During winter a temperature of geothermal water is decreasing to 65°C, while the average summer temperature is around 82°C. Similarly, the mass flow rates are varying in the range from 0.05 to 1 kg/h. The goal is to determine the operating point of the pump (frequency) and position of the control valve (hydraulic resistance) in order to maximize the profit of the plant (Eq. (22)).

The simulation constraints are given in the form of physical limitations concerning the frequency range from 15 to 50 Hz and the range of valve hydraulic resistance 4.66 to 300. In addition to optimization constraints presented by Eqs. (25)–(27), an additional limitation has been introduced regarding the cavitation of the ejector operation represented by the equation:

$$p_{103} < p_{107,cavitation} + 1500\text{Pa} \quad (29)$$

where  $p_{107,cavitation}$  is the saturation pressure of operating water for temperature  $t_{107}$ .

The maximum number of iterations was held fixed ( $ITER_{max} = 100$ ). Simulations were performed at three

temperatures 65°C, 73.5°C and 82°C. For each temperature, the mass flow rate has been varied from 0.05 to 1 kg/s, with a step of 0.05 kg/s. Other parameters of antlion algorithm have been set as shown in the study by Mirjalili [24].

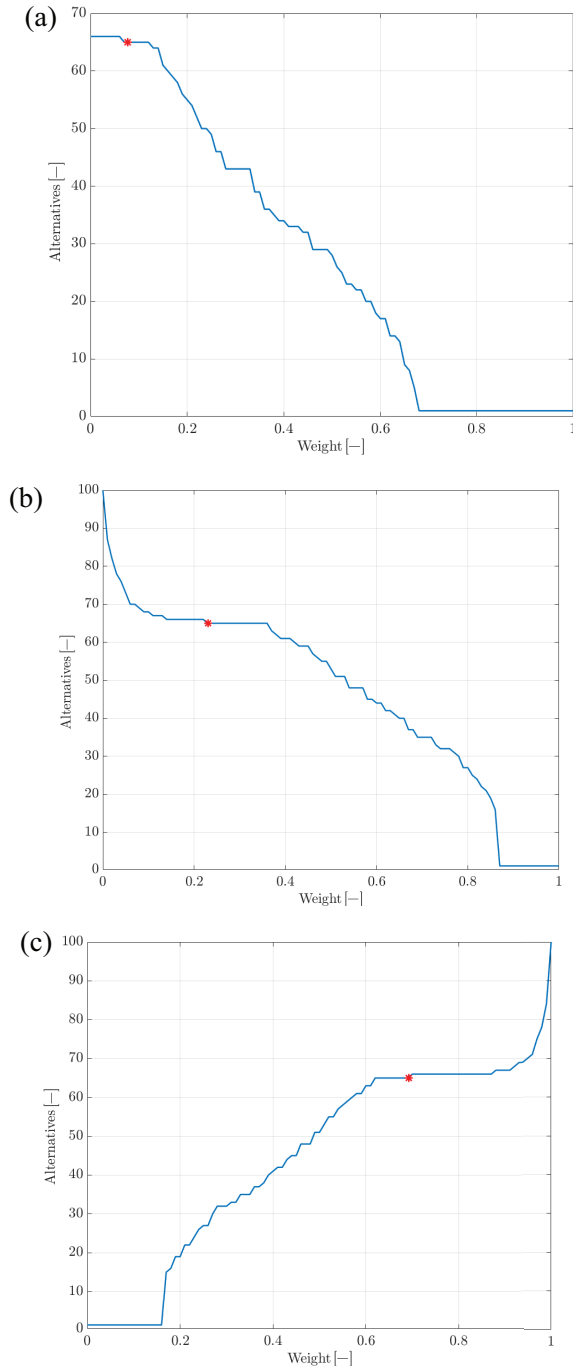


Fig. 5. Sensitivity analysis of MCDM: (a) EXloss, (b) investment and (c) profit. It can be observed that for values of high-profit weights, the optimal decision tends to the alternatives with highest investment cost. Also, the higher weights values of investment and exergy losses lead to low production of desalinated water. Alternative 65 is robust, that is, in a wide range of movements, the weight of profit, investment and exergy losses does not change.

Simulation of the process in a steady state has been made in accordance with the equations for mass and energy balances of each individual part of the plant.

### 3.3.1. Pump—PUI

Based on calculations for the individual parts of the plant (Table 4) and constant thermophysical states of water desalination plant (Table 1) the following pump is chosen: Grundfos NK 125-250/222 A2-FAE-BAQE. Pump characteristic is shown in Fig. 6(a) (continuous blue line).

Data obtained from the manufacturer are given as a discrete set of values and only for one frequency. The data are fitted for a variety of frequencies by linear regression (Furrier's second-order method) evaluated as follows:

Table 4  
Geometric sizes of individual parts of plant equipment

$A_{\text{nozzle}}$ , m <sup>2</sup>	0.0038
$A_{\text{nozzle}}/A_{\text{chamber}}$	0.19183
$L$ , m	10
$S_{\text{HE}}$ , m <sup>2</sup>	10
$D$ , m	0.2588
$S_j$ , m	0.01
$ds$ , m	0.04

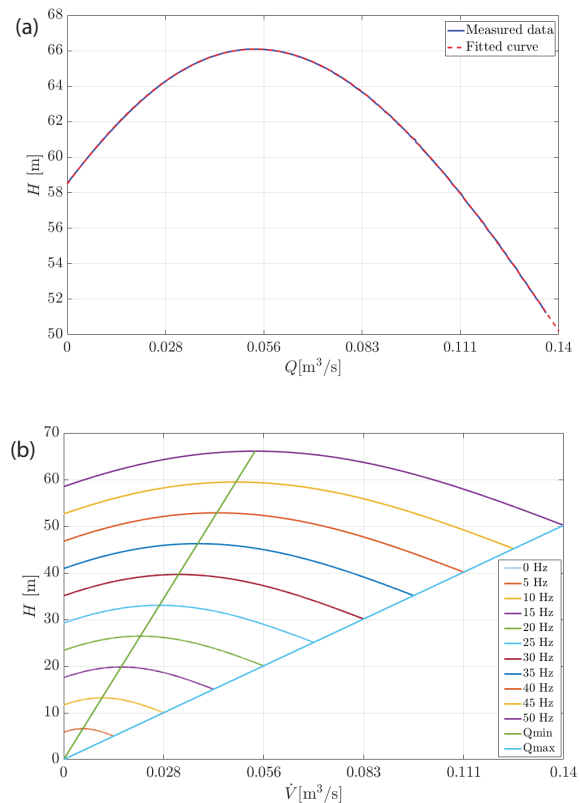


Fig. 6. (a) Actual pump characteristics (from manufacturer) and (b) fitted pump characteristics for  $t_w = 346.65$  K,  $\rho_w = 975.7$  kg/m<sup>3</sup> and  $f = 50$  Hz.

$$y = a_0 + a_1 \cos(\omega x) + b_1 \sin(\omega x) + a_2 \cos(2\omega x) + b_2 \sin(2\omega x) \quad (30)$$

where  $a_0 = 47.31$ ,  $a_1 = 10.711$ ,  $a_2 = 0.4696$ ,  $b_1 = 15.27$ ,  $b_2 = 0.2751$  and  $\omega = 0.004719$ .

The spectre of pump characteristics for different frequencies, which drives the pump, is given in Fig. 6(b). Due to the motor's frequency limitation and cavitation, the pump cannot work at every point represented in the diagram. Therefore, minimal and maximal possible values are labeled as  $Q_{\min}$  and  $Q_{\max}$ .

### 3.3.2. Ejector—E1

Simulation equations of the liquid jet vacuum ejector (Eqs. (10) and (11)) are given in accordance with the semi-experimental equations shown in the study by Sokolov [26].

$$q = \dot{m}_{101} \cdot \frac{(h_{101} - h_{102})}{(h_{103} - h_{102})} \cdot \frac{1}{\rho_{103} \cdot V_{107}} \quad (31)$$

$$\frac{p_{104} - p_{103}}{p_{107} - p_{103}} = 1.75 \cdot \frac{A_{\text{nozzle}}}{A_{\text{chamber}}} - 1.07 \cdot \left( \frac{A_{\text{nozzle}}}{A_{\text{chamber}}} \right)^2 \cdot \left( 1 + \frac{q}{15} \right)^2 \quad (32)$$

where  $(\dot{V}_{107}, p_{107}) = F(f, \zeta_v)$ .

### 3.3.3. Heat exchanger—HE1

The design of the heat exchanger is based on the energy balance equation and the system of equations for calculation of the overall heat transfer coefficient as a basis for using the NTU method [30]. The flow rate of the cold fluid (river water) is assumed to be infinite; so there will be no change of the cold fluid temperature (it is equal to the ambient temperature)—consequently  $R = \infty$ . By adopting the expression for the mean value of the Nusselt numbers, on the desalinated water side (Eq. (33)) [31], and on the river water side (Eq. (34)) [32], the desired temperature  $t_{105}$  can be determined based on the adopted surface and given states  $t_{104}$ ,  $p_{104}$  and  $t_{\text{amb}}$ .

$$\text{Nu}_D = 0.027 \cdot \text{Re}_D \cdot \text{Pr}^{\frac{1}{3}} \cdot \left( \frac{\mu}{\mu_s} \right)^{0.14} \quad (33)$$

$$\text{Nu}_{\text{river}} = a_1 \cdot \left( 1.33 \cdot \frac{d_s}{S_c} \right)^a \cdot \text{Re}_{\text{river}}^{a_2} \cdot \text{Pr}^{\frac{1}{3}} \cdot \phi_t \quad (34)$$

where  $\text{Re}$  is Reynolds number;  $\text{Pr}$  is Prandtl number;  $\text{Nu}_{\text{river}}$  and  $\text{Nu}_D$  are the Nusselt numbers of the cold fluid (river) and hot fluid (desalinated water), respectively;  $\phi_t = (T/T_w)^{0.25}$  is the correction factor;  $a_1$  and  $a_2$  are experimental parameters;  $d_s$  is the external pipe cross section; and  $S_c$  is the distance between the pipes.

Although the fouling factor plays an important role on performances of heat exchangers, as it has been shown in the

studies by Genić et al. [33] and Milanovic et al. [34], in this paper they have been chosen to disregard the fouling.

### 3.4. Optimization results and discussion

The results of the plant optimization for different values of mass flow rates at the plant's inlet ( $\dot{m}_{101}$ ) and temperatures ( $t_{101}$ ) are presented in Figs. 7 and 8. It can be observed (Fig. 7) that on the optimal trajectory, vapour pressure of entrained steam ( $p_{103}$ ) and corresponding temperature ( $t_{103}$ ) are increasing with the increase of  $\dot{m}_{101}$  and  $t_{101}$ . In addition, the mass flow rate of the desalinated water  $\dot{m}_{103}$  (Fig. 8(a)) along with the motive water pressure  $p_{107}$  and the mass flow rate  $\dot{m}_{107}$  (Figs. 8(b) and (e), respectively) are increasing with the increase of  $\dot{m}_{101}$  and  $t_{101}$ . The temperature distribution on the optimal trajectory at the ejector and the heat exchanger outlet  $t_{104}$  and  $t_{101}$ , respectively, are presented in Figs. 8(d) and (c). The smoothness of the optimal trajectory is not guaranteed because of the constraints and applied heuristics. The change of the maximum profit of the plant with the  $\dot{m}_{101}$  and temperature  $t_{101}$  is presented in Fig. 9. It could be concluded that the larger values of the plant's inlet mass flow rates  $\dot{m}_{101}$

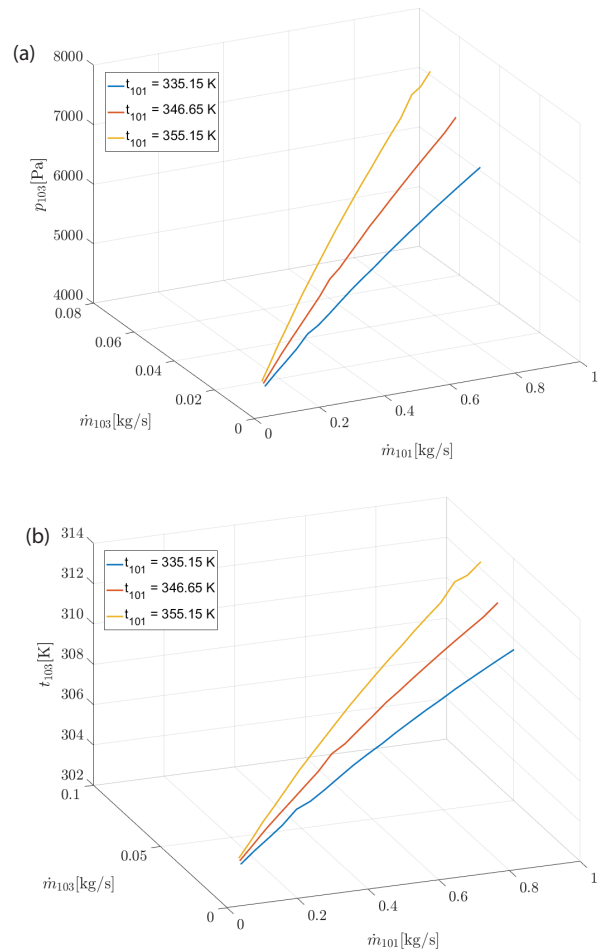


Fig. 7. Optimal trajectory at three temperatures  $t_{101}$ . Change in (a) temperature  $t_{103}$  and (b) pressure  $p_{103}$  in vessel P1. Figure shows that on the optimal trajectory, pressure  $p_{103}$  and corresponding temperature  $t_{103}$  are increasing with the increase of  $\dot{m}_{101}$  and  $t_{101}$ .

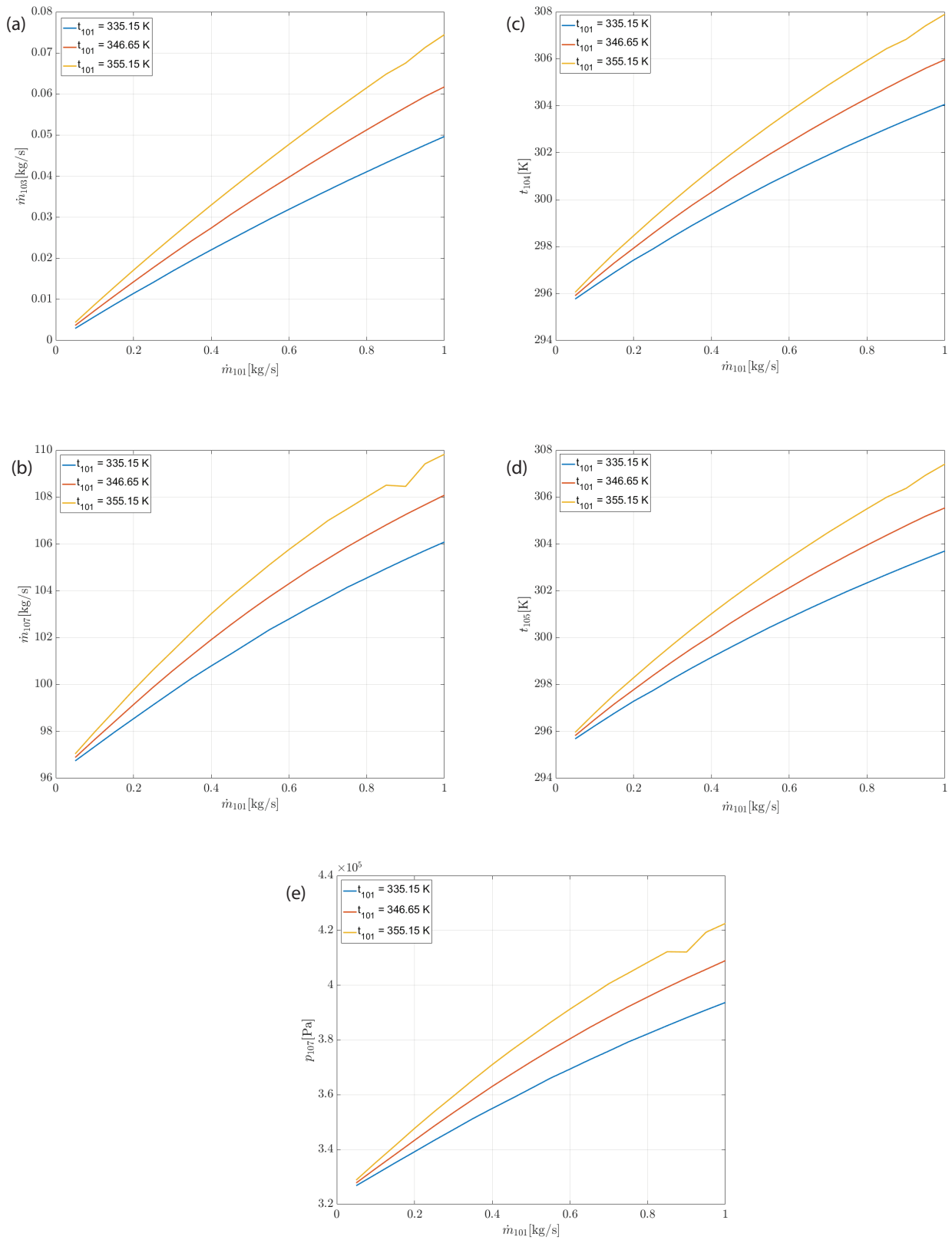


Fig. 8. Dependence of (a)  $\dot{m}_{103}$  (b)  $\dot{m}_{107}$  (c)  $t_{104}$  (d)  $t_{105}$  and (e)  $p_{107}$  with respect to mass flow rate  $\dot{m}_{101}$ . Positive correlation can be observed between mass flow rate  $\dot{m}_{103}$ , mass flow rate of the desalinated water  $\dot{m}_{103}$ , motive water pressure  $p_{107}$  and mass flow rate  $\dot{m}_{107}$ . Higher temperatures  $t_{101}$  lead to the lower values of pressure  $p_{107}$  for equal mass flow rates of desalinated water.

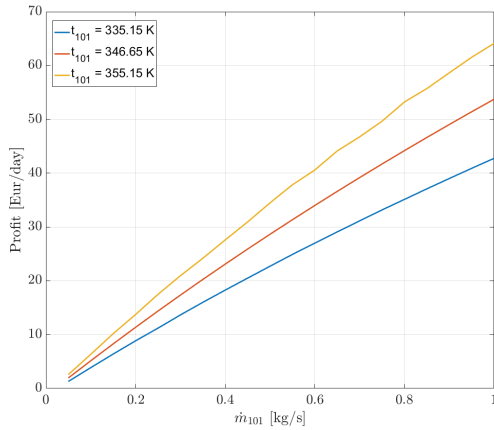


Fig. 9. Cost functions of single-objective optimization. The larger values of plant's inlet mass flow rate  $\dot{m}_{101}$  (and temperature  $t_{101}$ ) correspond to the higher profits and operational costs.

and temperatures  $t_{101}$  are corresponding consequently to the higher profits and operational costs.

#### 4. Control

Control strategy and controller design based on nonlinear dynamical model are presented in this section. A nonlinear model of the plant is presented along with simulation results in Subsection 4.1. Control strategy and linearization of the nonlinear model are presented in subsections 4.2 and 4.3, respectively. The latter subsections have been concerned with linear and nonlinear gain-scheduled controller design.

##### 4.1. Modeling and simulation

In order to acquire a suitable dynamical model for the control purposes, as shown in Fig. 3, the following assumptions are introduced:

- The specific heat capacities of liquid at constant pressure ( $c_p$ ) and constant volume ( $c_v$ ) are constant;
- Volumes occupied by vapour ( $V_v$ ) and liquid ( $V_L$ ) are constant;
- Steady-state conditions of liquid jet vacuum ejector are assumed;
- Mass accumulation in vessel V1 is negligible;
- Water density is constant;
- Water vapour is saturated at the position 103, whereas liquid is boiled at the position 102 such that,  $p_{103} = p_{102}$  and  $t_{103} = t_{102}$ .

Based on the volume ER, (Eq. (31)) and semi-empirical (Eq. (32)) mass flow rate  $\dot{m}_{103}$  can be expressed as follows:

$$\dot{m}_{103} = \left( \frac{1.75 \cdot \frac{A_{\text{nozzle}}}{A_{\text{chamber}}} \frac{p_{104} - p_{102}}{p_{107} - p_{102}}}{1.07 \cdot \left( \frac{A_{\text{nozzle}}}{A_{\text{chamber}}} \right)^2} - 1 \right) \frac{15 \cdot \dot{m}_{107} \rho_{103}}{\rho_{107}} \quad (35)$$

where  $(p_{107}, \dot{m}_{107}) = F(\zeta, f)$ .

Mass and energy conservation equations for the vessel P1 are presented respectively by the following equations:

$$\dot{m}_{101} = \dot{m}_{102} + \dot{m}_{103} \quad (36)$$

$$\begin{aligned} \frac{d}{dt} (\rho_L \cdot V_L \cdot c_{vL} \cdot t_{102} + \rho_V \cdot V_V (c_{vL} \cdot t_{102} + \Delta h_{\text{LAT}})) \\ = \dot{m}_{101} \cdot c_{pL} \cdot t_{101} - \dot{m}_{102} \cdot c_{pL} \cdot t_{102} - \dot{m}_{103} (c_{pL} \cdot t_{102} + \Delta h_{\text{LAT}}) \end{aligned} \quad (37)$$

Vapour density and latent heat are expressed by the following equations:

$$\rho_V = D_1 \cdot t_{102}^3 + D_2 \cdot t_{102}^2 + D_3 \cdot t_{102} + D_4 \quad (38)$$

$$\Delta h_{\text{LAT}} = b_1 \cdot t_{102} + b_2 \quad (39)$$

where  $D_1, D_2, D_3, D_4, b_1$  and  $b_2$  are regression coefficients.

After simplification, the following expression is obtained:

$$\frac{dt_{102}}{dt} = \frac{\dot{m}_{101} \cdot c_{pL} \cdot (t_{101} - t_{102}) - \dot{m}_{103} \cdot \Delta h_{\text{LAT}}}{C} \quad (40)$$

$$\begin{aligned} C = V_L \cdot \rho_L \cdot c_{vL} + V_V \cdot ((D_4 \cdot B_1 + b_2 \cdot D_3) + 2 \cdot t_{102} \cdot (D_3 \cdot B_1 + b_2 \cdot D_2) \\ + 3 \cdot t_{102}^2 \cdot (D_2 \cdot B_1 + b_2 \cdot D_1) + 4 \cdot t_{102}^3 \cdot D_1 \cdot B_1) \end{aligned} \quad (41)$$

where  $B_1 = b_1 + C_{pL}$ .

The simulation has been performed using a combination of the Eqs. (35) and (41). Initial conditions were  $t_{102}^0 = t_{101}$ , and the plant is considered to be in steady state with PU1 turned off. In addition, the simulation diagram of the plant is shown in Fig. 10.

Numerical simulations of the nonlinear mathematical model are presented in Fig. 11. Simulations have been performed for step input and three different temperatures. One of the methods to verify dynamical model is to compare steady-state values from Fig. 7 with ones acquired through the simulation. It can be seen that the final values of dynamical simulation matches steady-state values from Fig. 7. Therefore, the presented dynamical model is considered accurate enough for control purposes.

##### 4.2. Control strategy

From Eqs. (35)–(41) and Fig. 11, it can be determined that the plant is stable for arbitrary input value. However, the steady-state values are suboptimal, time constants are too high and the tracking of the desired value is poor. Therefore, in order to improve the system performance a PI controller is introduced. Besides, following problems are occurring; firstly, the plant is highly nonlinear, and secondly, it cannot be linearized around some nominal operating point because the operating point is varying with the variation of the disturbances. Considering the latter, a feedback gain-scheduling controller is proposed (Fig. 12). The gains of the proposed

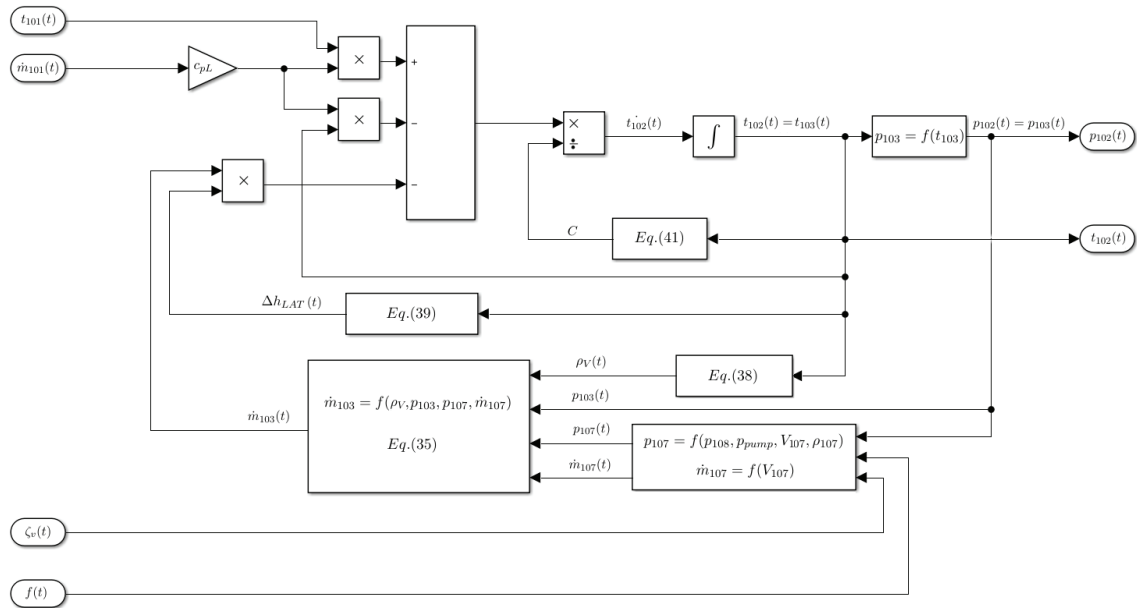


Fig. 10. Plant's simulation diagram.

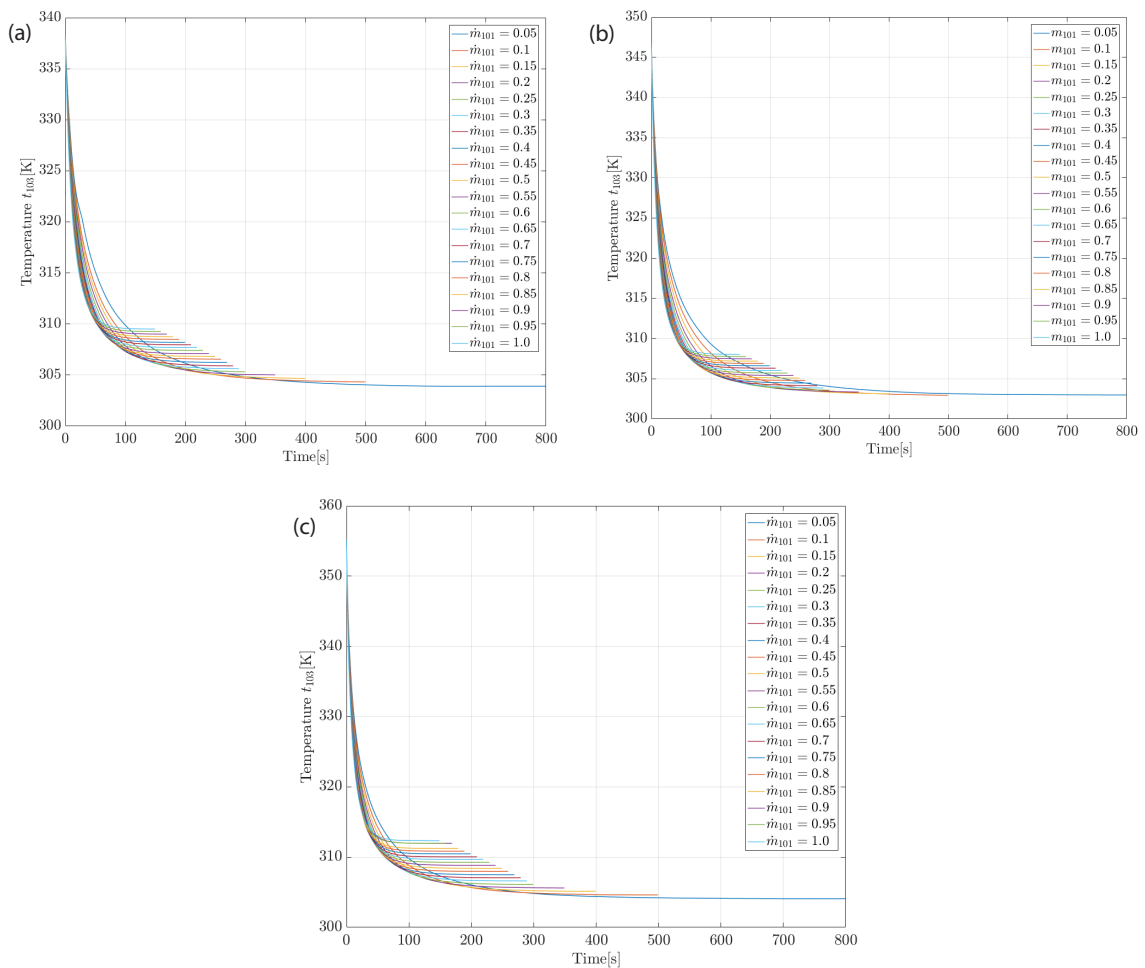


Fig. 11. Step responses of nonlinear plant model for every optimal operating point initiated with optimal values of  $f$  (Hz) and  $\zeta_v$ : (a)  $t_{101} = 335.15$  K, (b)  $t_{101} = 346.65$  K and (c)  $t_{101} = 355.15$  K.

controller are corrected as the disturbances vary. It should be noted that the presented controller will control the frequency of PU1, while hydraulic resistance V2 was controlled by the lookup table formed from Table 5.

Further, using the optimal values from Table 5, an optimal value lookup table is formed. Applying the linear interpolation on the optimal values from the lookup table, an optimal reference signal  $r(t)$  is acquired as a desired optimal trajectory (Fig. 7).

To obtain controller gains for each value of the disturbance, a linearized plant at the same operating point in which the optimum values are calculated is needed. Adjustment of the controller gains is occurring continuously as the disturbance changes, whereas the values between two data in lookup table are obtained by linear interpolation. Variations in the disturbances are influencing a change in the optimal reference signal. Hence, the controller is going

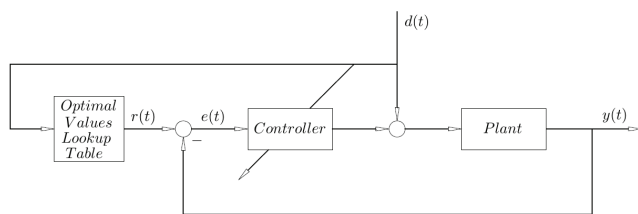


Fig. 12. General control system block diagram. Controller gains and reference signal  $r(t)$  are adjusted online according to the current disturbance signal  $d(t)$ .

Table 5  
Optimal values of  $f$  and  $\zeta_v$  for different inlet mass flow rates  $\dot{m}_{101}$  and temperatures  $t_{101}$

$\dot{m}_{101}$ (kg/s)	$t_{101} = 335.15$ K		$t_{101} = 346.65$ K		$t_{101} = 355.15$ K	
	$f$ (Hz)	$\zeta_v(-)$	$f$ (Hz)	$\zeta_v(-)$	$f$ (Hz)	$\zeta_v(-)$
0.05	35.21	75.05	36.34	86.10	35.13	72.01
0.10	41.51	136.53	35.29	69.29	35.67	71.01
0.15	35.47	69.03	35.57	66.95	35.85	66.56
0.20	36.94	80.12	42.27	129.34	36.12	63.07
0.25	35.94	65.66	42.58	126.5	36.67	62.79
0.30	36.69	69.32	39.27	88.81	36.66	57.28
0.35	36.39	62.35	36.62	58.03	37.03	55.53
0.40	36.67	61.58	36.87	56.10	37.15	51.64
0.45	36.59	57.43	40.13	83.07	37.51	50.41
0.50	38.19	69.55	44.00	114.58	38.03	50.96
0.55	36.96	54.21	38.12	56.15	38.28	49.01
0.60	37.24	53.94	37.78	49.47	38.40	46.13
0.65	40.33	80.03	37.85	46.66	38.82	46.21
0.70	37.79	53.38	38.34	47.98	40.21	54.69
0.75	37.60	48.75	41.37	71.97	39.01	41.18
0.80	40.87	76.30	38.58	44.18	39.38	41.38
0.85	38.63	53.25	38.80	43.38	39.53	39.75
0.90	44.87	106.45	38.92	41.82	39.08	36.06
0.95	38.27	45.24	39.01	40.14	39.74	36.29
1.00	39.81	56.78	46.14	98.22	39.98	35.97

to be tuned to have good reference tracking characteristic, thus, the integral absolute error (IAE) should be as smallest as possible.

#### 4.3. Linearization

In order to tune the gain-scheduled controller, as it has been evaluated in Subsection 4.2, the linear model in each optimization point is necessary.

From Figs. 10 and 11, it can be concluded that the plant can be represented as the first-order linear system around the desired operating point described as follows:

$$G_p(s) = \frac{K}{1 + sT} \quad (42)$$

where  $K$  represents process gain,  $T$  is time constant and  $s$  is Laplace operator.

Optimal values of  $f$  and  $\zeta_v$  from Table 5 are adopted for step initialization. The nonlinear step response model was obtained by simulating step responses using a simulation diagram (Fig. 10).

Obtained nonlinear step responses are linearized by calculating time constant  $T(s)$  and gain  $K(-)$  of the first-order process for every operating point. Hence, the plant was linearized in 20 operating points per an optimized temperature. The results of linearization are shown in Fig. 13.

This simple yet effective method can be verified by comparing nonlinear and linearized step responses. In Fig. 14, the comparison was shown only for three operating points per optimized temperature. Because the ejector has a highly nonlinear dynamic, this results is considered to be accurate enough to calculate controller parameters.

#### 4.4. Gain-scheduling proportional integral control (GSPI)

Gain-scheduling controllers are one of the most popular approaches for nonlinear control design. It has been used successfully in various industries especially in process control. Because the PID controller is the most used conventional controller, and therefore PI as a particular case, it is the logical first choice of the controller for the stable plant.

The optimal reference signal, gains of the PI controller and optimal hydraulic resistance  $\zeta_v$  are acquired by using lookup tables and measuring the disturbances. Error signal,  $e(t)$ , is formed as a difference between an optimal reference signal,  $r(t)$ , and plant output,  $y(t)$ , as it can be seen in Fig. 15.

It is shown that the plant can be represented as a series of linearized first-order linear ordinary differential equations. Henceforth using the Laplace transformation, the system will have the general form (Eq. 42).

Adopting PI regulator can be expressed as follows:

$$g_c(t) = K_p e(t) + K_i \int_0^t e(\tau) d\tau \quad (43)$$

where  $e$  is error signal,  $K_p$  and  $K_i$  are PI gains, respectively.

By applying the Laplace transform on controller transfer function is obtained:

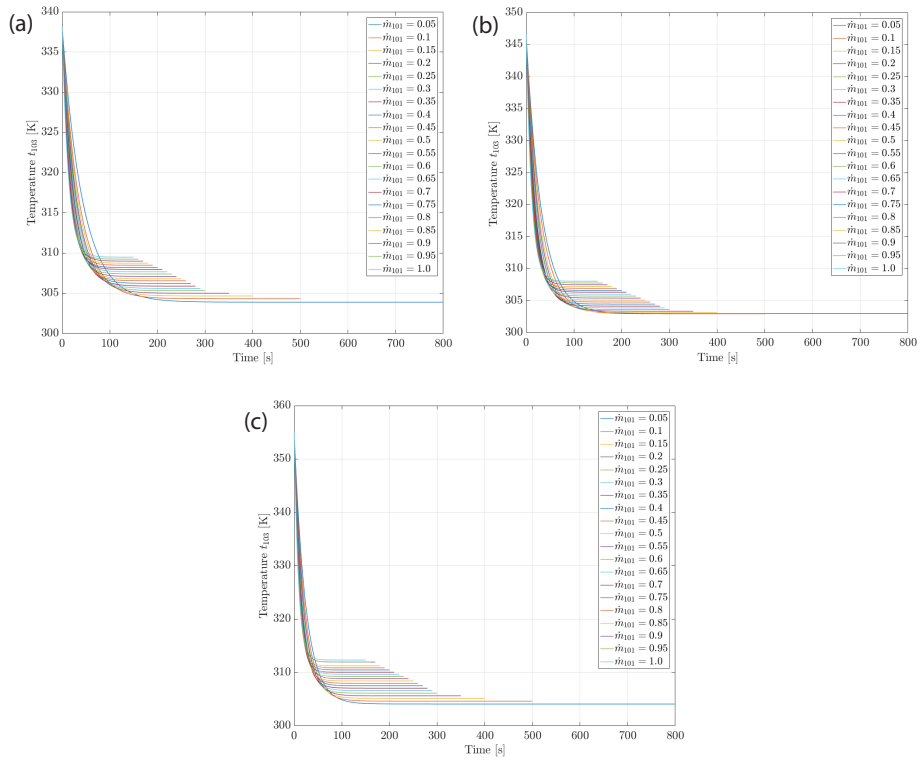


Fig. 13. Step response of linearized plant model for every optimal operating point initiated with optimal values of  $f(\text{Hz})$  and  $\zeta_v(-)$ : (a)  $t_{101} = 335.15$  K, (b)  $t_{101} = 346.65$  K and (c)  $t_{101} = 355.15$  K.

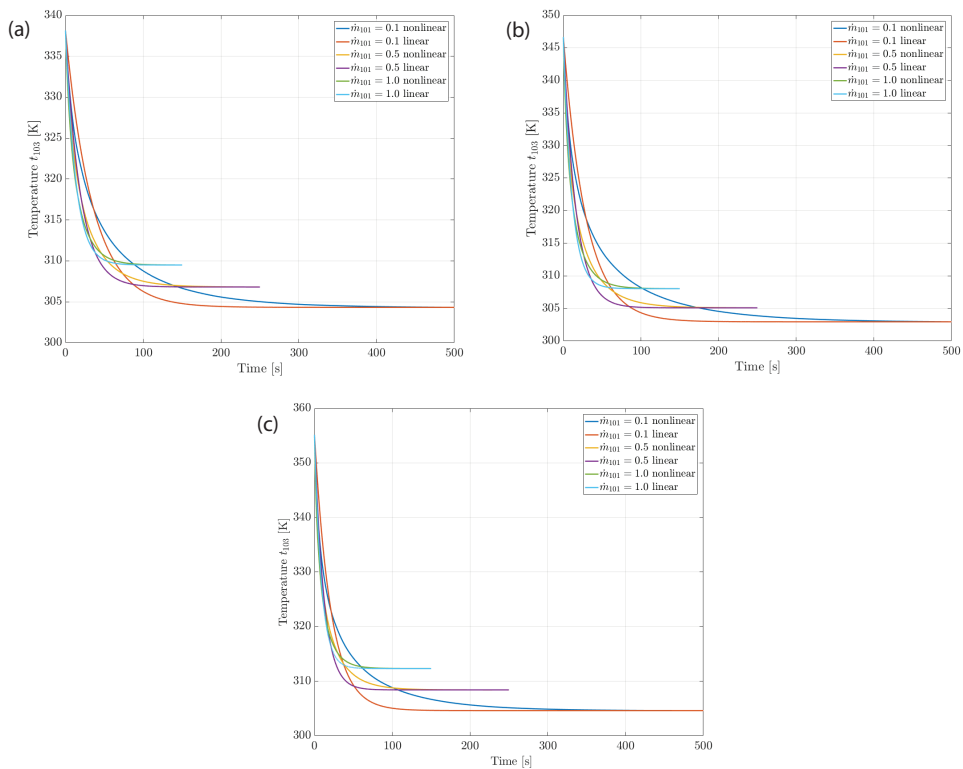


Fig. 14. Step responses of nonlinear and linearized plant model for three optimal operating points initiated with optimal values of  $f(\text{Hz})$  and  $\zeta_v(-)$ .

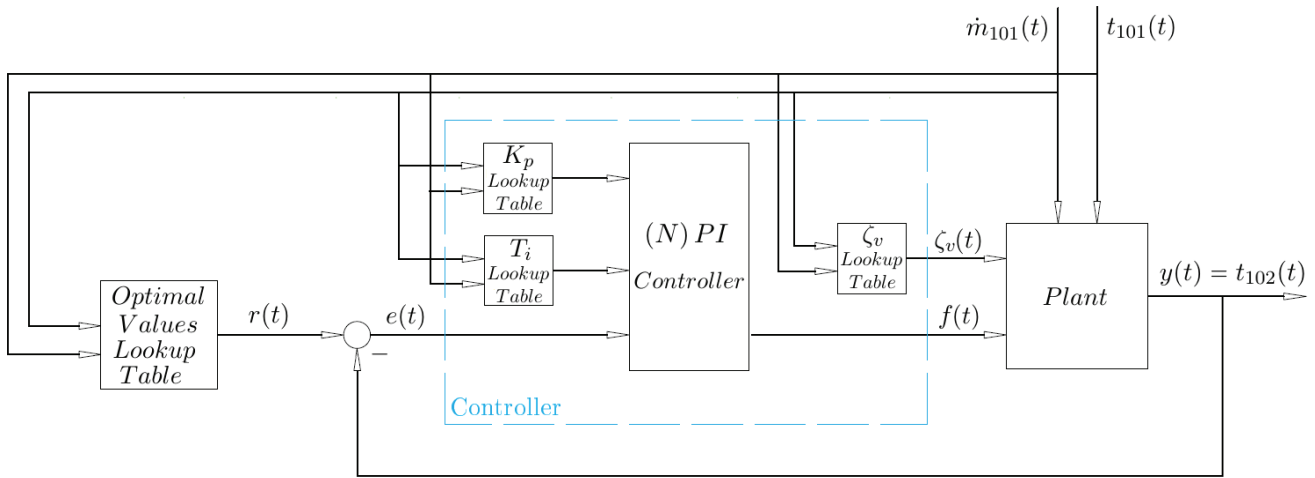


Fig. 15. Block diagram of the proposed control system.

$$G_c(s) = K_c \left( 1 + \frac{1}{sT_i} \right) \tag{44}$$

where  $K_c$  is controller gain and  $T_i$  is integral time.

After adding the feedback controller to linearized plant the closed-loop system will have second-order form as follows:

$$G(s) = \frac{1}{\frac{s^2}{\omega_0^2} + \frac{2\zeta s}{\omega_0} + 1} \tag{45}$$

where  $\omega_0$  is natural frequency and  $\zeta$  is damping ratio.

Therefore, having the second-order system, it is possible to place poles of the closed-loop system by changing the controller parameters to obtain the desired relative dumping,  $\zeta$ , and natural frequency of poles,  $\omega_0$  as it is evaluated in the study by Åström and Hägglund [35]:

$$K_c = \frac{2\zeta\omega_0 T - 1}{K} \tag{46}$$

$$T_i = \frac{2\zeta\omega_0 T - 1}{\omega_0^2 T} \tag{47}$$

Considering Eqs. (42) and (44), system transfer function can be presented as follows:

$$G(s) = \frac{G_p(s)G_c(s)}{1 + G_p(s)G_c(s)} \tag{48}$$

where open-loop transfer function is expressed as follows:

$$L(s) = G_p(s)G_c(s) \tag{49}$$

Eq. (49) can be further developed by applying Eqs. (42) and (44):

$$L(s) = \frac{K}{1 + sT} \cdot \left( K_c + \frac{K_c}{sT_i} \right) = \frac{KcK(sT_i + 1)}{s^2TT_i + sT_i} \tag{50}$$

Applying Fourier transformation to Eq. (50) (formally  $s = j\omega$ ) phase margin (PM) can be calculated as follows:

$$PM = \pi + \angle L(j\omega) \tag{51}$$

Controller gains are tuned utilizing Eqs. (46), (47) and (51) bearing in mind that all tuned linearized plants have the same PM, dumping,  $\zeta$ , and overshoot (OS) (%), as it is shown in Table 6.

#### 4.5. Gain-scheduling nonlinear proportional integral control (GSNPI)

To improve tracking performance of system, the nonlinear PI controller with the variable gains are introduced. Improvement of the conventional to a nonlinear PID controller is based on the way that controller interprets the error signal. The idea is to make the controller more sensitive for smaller error signals and less sensitive for larger error signals [36,37].

The proposed nonlinear modification of error signal is given by the following equation and Fig. 16:

$$e_c(t) = \text{sign}(e(t))|e(t)|^{1/2} \tag{52}$$

Modified PID controller has the following form:

$$G_c(s) = K_p e_c(t) + K_i \int_0^t e_c(\tau) d\tau + K_d \dot{e}_c \tag{53}$$

thus, modified PI is as follows:

$$G_c(s) = K_p e_c(t) + K_i \int_0^t e_c(\tau) d\tau \tag{54}$$

Table 6  
Comparison of simulated controllers by IAE, ITAE, ISE and ITSE criteria

No.	Controller	Phase margin (°)	Damping $\zeta_v(-)$	Overshot (%)	IAE	ITAE	ISE	ITSE
1	GSI	30	0.536	13.6	1233.0	$3.218 \cdot 10^5$	25410.0	$1.833 \cdot 10^8$
2	GSI	45	0.536	13.6	1220.0	$3.211 \cdot 10^5$	25400.0	$1.833 \cdot 10^8$
3	GSPI	60	0.577	10.8	398.6	$7.81 \cdot 10^4$	6110.0	$1.048 \cdot 10^7$
4	GSNPI	60	0.577	10.8	351.7	$2.188 \cdot 10^4$	5621	$9.642 \cdot 10^6$
5	GSI	–	0.642	8.8	1490.0	$3.9302 \cdot 10^5$	22381	$3.482 \cdot 10^7$
6	GSPI	70.4	0.707	4.3	413.2	$8.593 \cdot 10^4$	6399.0	$1.328 \cdot 10^7$
7	GSPI	70.5	0.709	4.3	407.6	$8.4765 \cdot 10^4$	6408.0	$1.303 \cdot 10^7$
8	GSPI	75	0.772	2.2	443.7	$9.15 \cdot 10^4$	6999.0	$1.49 \cdot 10^7$
9	GSPI	80	0.850	0.6	499.1	$9.985 \cdot 10^4$	7886.0	$1.767 \cdot 10^7$
10	GSPI	90	1	0	689.7	$1.262 \cdot 10^5$	10660.0	$2.698 \cdot 10^7$
11	PI	60	$K_p = -1.10375$	$T_i = -5.331$	432.7	$8.641 \cdot 10^4$	8912	$1.672 \cdot 10^7$

GSI – Gain schedule integral.

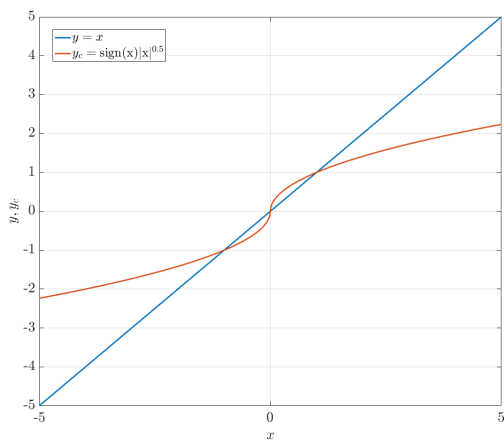


Fig. 16. Linear and nonlinear gains. Linear controller gain (blue) passes the error value to the controller, on the other hand, nonlinear gain (red) is passing penalized values for large error signals and gained values for smaller error signals.

The same parameters were used for both GSPI and GSNPI controllers and they are tuned on the manner already explained in Subsection 4.4.

### 5. Simulation results

Variety of controllers derived from PID have been tested by extensive simulation. Simulations have been performed for initial conditions  $t_{102}^0 = 355.15\text{K}$ . Change in the disturbances was chosen to simulate real-life worst-case scenario, where mass flow rate  $m_{101}$  drops and temperature  $t_{101}$  rises over a period of 1,000 s, as shown in Fig. 17. Nonlinear differential equations have been solved using variable step ODE45 solver in Matlab/Octave program package. The nonlinear algebraic equation has been solved using the bisection method.

Performances of the controllers have been compared using following criteria: IAE, integral time absolute error (ITAE), integral square error (ISE) and integral time square error (ITSE) [35].

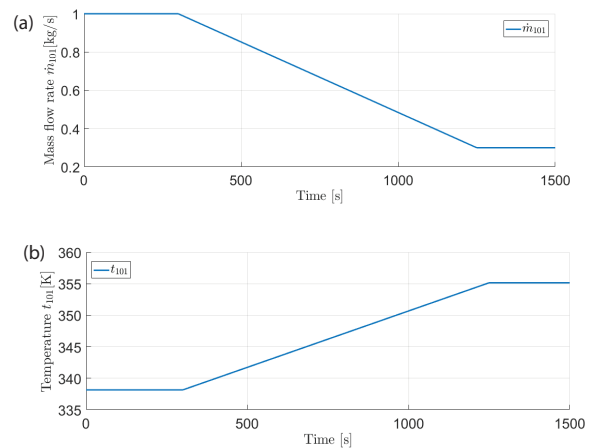


Fig. 17. Time change of input temperature  $t_{101}$  and mass flow rate  $m_{101}$  during 1,500 s of simulation.

The comparison is given in Table 6. It can be seen that the best results were obtained by utilizing GSPI and GSNPI controllers with parameters calculated for the following performance: PM = 60,  $\zeta = 0.577$  and OS = 10.8%. Lookup table of GSPI controllers gains for  $K_c$  and  $T_i$  is given in Figs. 18(a) and (b), respectively.

Simulation results for GSPI and GSNPI controllers are given in Fig. 19. It is to be noted that the nonlinear controller needs more time to place the system in the vicinity of the optimal trajectory. The reason for this behavior is the penalization of the error signal for larger differences between the reference signal and the process value. Although both gain-scheduling controllers have similar control trajectories (Fig. 20), the nonlinear controller has better reference tracking, which can be concluded due to the difference in error signals (Fig. 21). Because the references derived from the lookup table present the optimal trajectory of the system, superb reference tracking is necessary. Therefore, this justifies the use of GSNPI controller for this type of systems.

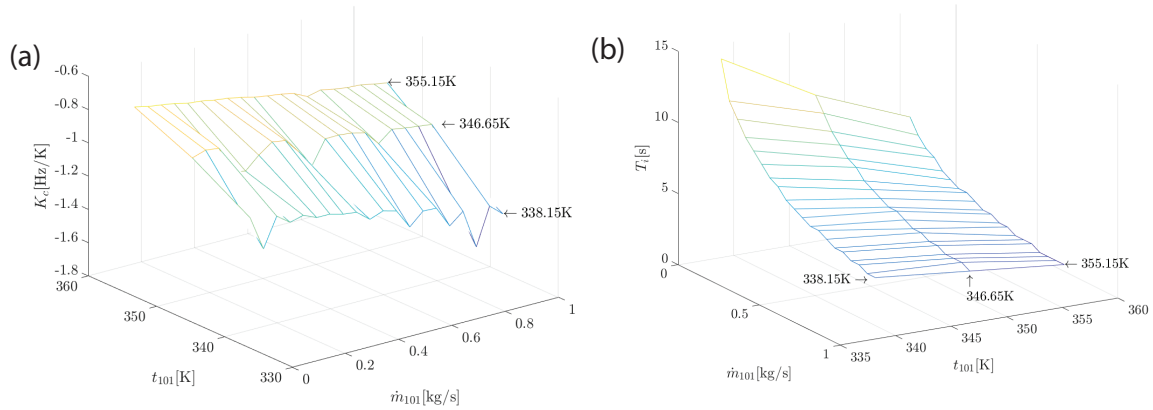


Fig. 18. Surface of tuned parameters of GS(N)PI controller for all evaluated values of  $\dot{m}_{101}$  and  $t_{101}$ : (a) controller gain  $K_c$  and (b) integral time  $T_i$ .

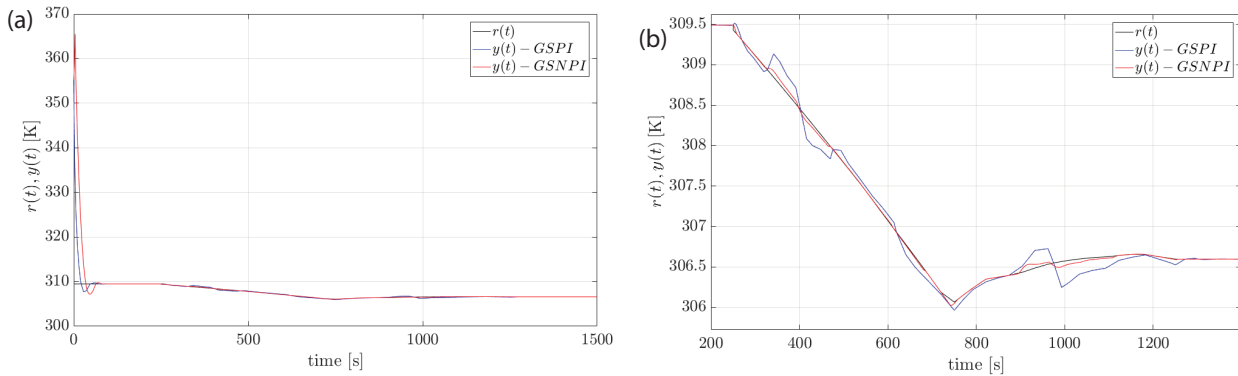


Fig. 19. (a) Simulation of nonlinear system controlled by the gain scheduling PI and nonlinear PI controller under the influence of disturbances, with initial condition  $t_{102} = 355.15$  K. Penalization of error signal causes GSNPI to be slower than GSPI when the error signal is larger. (b) Close-up look on the area where disturbance is taking place. It can be noted that GSNPI has better reference tracking than GSPI controller.

**6. Conclusion**

This paper gives a novel approach for modeling, simulation and control of a thermal VC water desalination plant with liquid jet vacuum ejector. In the nominal regime, the optimal plant design is obtained by performing both MOP (NSGA-II), with respect to total investment costs and profit, and MCDM (AHP and SAW method). Due to variations of temperatures and mass flow rates with seasons, simulations of the plant have been performed for different values of inlet boundary conditions. Based on the single-objective optimization (antlion algorithm) profit is maximized for a wide variety of inlet mineral water mass flow rates and temperatures. Additionally, in order to govern the plant through optimal thermodynamic states gain-scheduling controllers were designed. Moreover, different controllers have been compared. It has been shown that the best performance can be achieved by utilizing GSNPI. The GSPI can be used for engineering purposes due to more straightforward implementation.

Future studies of this multi-disciplinary research subject involve the use of different optimization and MCDM algorithms along with more advanced controllers such as

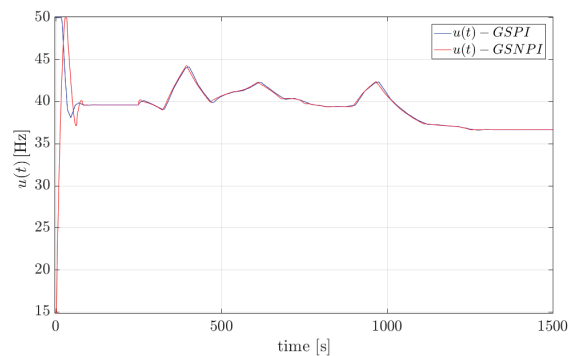


Fig. 20. Control signal  $u$ , generated by GSPI and GSNPI during simulation. Figure shows that although both controllers have similar control trajectories GSPI slightly more utilize the pump PU1. Therefore, it can be said that GSNPI controller is more optimal.

a model predictive controller. Development of an online optimizer coupled with an advanced controller is also a possibility.

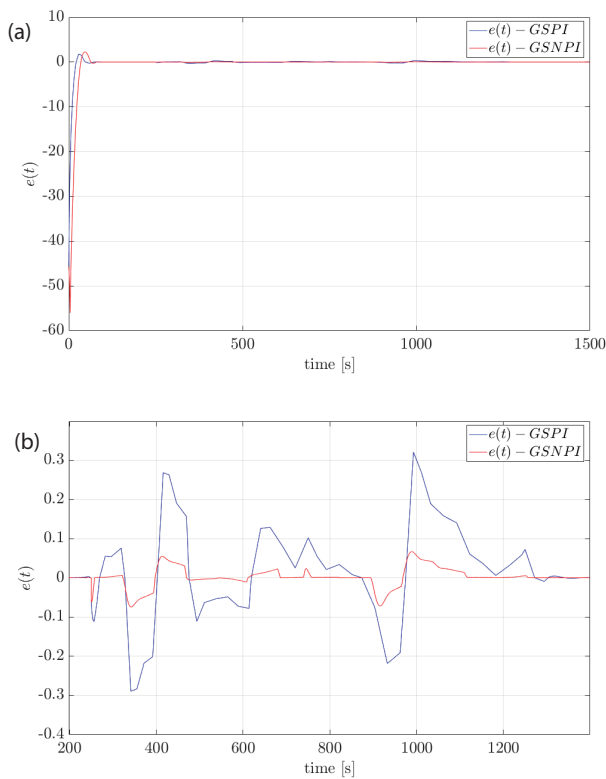


Fig. 21. (a) Error signal  $e$ , generated by GSPI and GSNPI during simulation. In the beginning of the simulation, GSPI controller faster places error signal in the vicinity of 0. (b) Close-up view of the error signal on the area where disturbance is taking place. During the process of desalination, GSNPI controller is better in guiding the process trough optimal states, thus, the error has the smaller values than with GSPI controller.

**Symbols**

$t$	—	temperature, K
$p$	—	Pressure, Pa
$h$	—	Enthalpy, J
$Q$	—	Total heat transfer, W
$\dot{m}$	—	Mass flow rate, kg/s
$\dot{V}$	—	Volumetric flow rate, m <sup>3</sup> /s
$c_p$	—	Specific heat capacity at constant pressure, J/kg K
$c_v$	—	Specific heat capacity at constant volume, J/kg K
$A$	—	Cross-section area, m <sup>2</sup>
$L$	—	Pipe length between pump and ejector inlet, m
$D$	—	Pipe diameter, m
$V$	—	Volume, m <sup>3</sup>
$d_s$	—	Diameter of heat exchanger tube, m
$\dot{S}_{HE}$	—	Heat transfer area, m <sup>2</sup>
$Re$	—	Reynolds number, —
$Pr$	—	Prandtl number, —
$Nu$	—	Nusselt number, —
$f$	—	Frequency, Hz
profit	—	Installation profit, EUR
EXloss	—	Exergy destruction, W

*Greek*

$\rho$	—	Density, kg/m <sup>3</sup>
$\zeta$	—	Hydraulic resistance of the valve, —
$\tau$	—	Time of integration
$\varphi$	—	Correction factor

*Subscripts*

$V$	—	Vapour
$L$	—	Liquid
$w$	—	Water
LAT	—	Latent
in	—	Inlet
out	—	Outlet
amb	—	Ambient
P1	—	Vessel 1
PU1	—	Pump 1
PU2	—	Pump 2
V1	—	Valve 1
V2	—	Valve 2
E1	—	Ejector
HE1	—	Heat exchanger 1
sat	—	Saturation
tot	—	Total

**References**

- [1] A. Reynaud, An econometric estimation of industrial water demand in France, *Environ. Resour. Econ.*, 25 (2003) 213–232.
- [2] P. Burek, Y. Satoh, Y. Wada, M. Floerke, S. Eisner, N. Hanasaki, D. Wiberg, Looking at the Spatial and Temporal Distribution of Global Water Availability and Demand, Vol. 18, EGU General Assembly Conference Abstracts, 2016, p. 16663.
- [3] A.D. Khawaji, I.K. Kutubkhanah, J. Wie, Advances in seawater desalination technologies, *Desalination*, 221 (2008) 47–69.
- [4] N. Ghaffour, T.M. Missimer, G.L. Amy, Technical review and evaluation of the economics of water desalination: current and future challenges for better water supply sustainability, *Desalination*, 309 (2013) 197–207.
- [5] H.M. Ettouney, H.T. El-Dessouky, *Fundamentals of Salt Water Desalination*, Elsevier, Amsterdam, 2002.
- [6] A. Gambier, A. Krasnik, E. Badreddin, Dynamic Modeling of a Simple Reverse Osmosis Desalination Plant for Advanced Control Purposes, American Control Conference, ACC'07, IEEE, 2007, pp. 4854–4859.
- [7] A. Abbas, N. Al-Bastaki, Modeling of an RO water desalination unit using neural networks, *Chem. Eng. J.*, 114 (2005) 139–143.
- [8] A. Gambier, A. Wellenreuther, E. Badreddin, Control system design of reverse osmosis plants by using advanced optimization techniques, *Desal. Wat. Treat.*, 10 (2009) 200–209.
- [9] B.D.H. Phuc, S. You, T. Lim, H. Kim, Modified PID control with  $H_\infty$  loop shaping synthesis for RO desalination plants, *Desal. Wat. Treat.*, 57 (2016) 25421–25434.
- [10] J.Z. Assef, J.C. Watters, P.B. Deshpande, I.M. Alatiqi, Advanced control of a reverse osmosis desalination unit, *J. Process Control*, 7 (1997) 283–289.
- [11] A.R. Bartman, P.D. Christofides, Y. Cohen, Nonlinear model-based control of an experimental reverse-osmosis water desalination system, *Ind. Eng. Chem. Res.*, 48 (2009) 6126–6136.
- [12] H.E. Fath, Solar distillation: a promising alternative for water provision with free energy, simple technology and a clean environment, *Desalination*, 116 (1998) 45–56.
- [13] H.B. Bacha, M. Bouzguenda, M.S. Abid, A.Y. Maalej, Modelling and simulation of a water desalination station with solar multiple condensation evaporation cycle technique, *Renewable Energy*, 18 (1999) 349–365.
- [14] M.I. Shatat, K. Mahkamov, Determination of rational design parameters of a multi-stage solar water desalination still using

- transient mathematical modelling, *Renewable Energy*, 35 (2010) 52–61.
- [15] H. Müller-Holst, M. Engelhardt, W. Schölkopf, Small-scale thermal seawater desalination simulation and optimization of system design, *Desalination*, 122 (1999) 255–262.
- [16] V.G. Gude, Geothermal source potential for water desalination—current status and future perspective, *Renewable Sustainable Energy Rev.*, 57 (2016) 1038–1065.
- [17] A.Z. Al-Garni, W.G. Abdelrahman, Water Desalination System using Geothermal Energy, March 22, 2016, US Patent 9,289,696.
- [18] E. Ahmetović, I.E. Grossmann, Z. Kravanjac, N. Ibrić, *Water Optimization in Process Industries*, 2016.
- [19] C.C. Coello, Evolutionary multi-objective optimization: a historical view of the field, *IEEE Comput. Intell. Mag.*, 1 (2006) 28–36.
- [20] K. Deb, A. Pratap, S. Agarwal, T. Meyarivan, A fast and elitist multiobjective genetic algorithm: NSGA-II, *IEEE Trans. Evol. Comput.*, 6 (2002) 182–197.
- [21] M.T. Jensen, Reducing the run-time complexity of multiobjective EAs: the NSGA-II and other algorithms, *IEEE Trans. Evol. Comput.*, 7 (2003) 503–515.
- [22] A. Ishizaka, A. Labib, Review of the main developments in the analytic hierarchy process, *Expert Syst. Appl.*, 38 (2011) 14336–14345.
- [23] A. Afshari, M. Mojahed, R.M. Yusuff, Simple additive weighting approach to personnel selection problem, *Int. J. Innovation Manage. Technol.*, 1 (2010) 511.
- [24] S. Mirjalili, The ant lion optimizer, *Adv. Eng. Software*, 83 (2015) 80–98.
- [25] I.H. Bell, J. Wronski, S. Quoilin, V. Lemort, Pure and pseudo-pure fluid thermophysical property evaluation and the open-source thermophysical property library coolprop, *Ind. Eng. Chem. Res.*, 53 (2014) 2498–2508.
- [26] E. Sokolov, *Flow Machines*, Moskva Energoatomizdat, Moscow, 1989 (in Russian).
- [27] R.K. Sinnott, G. Towler, *Chemical Engineering Design: SI ed.*, Elsevier, Lincare Hous, Jordan Hill, Oxford OX2 8DP, 2009.
- [28] W.D. Seider, J.D. Seader, D.R. Lewin, *Product and Process Design Principles: Synthesis, Analysis and Evaluation*, (With CD), John Wiley & Sons, 2009.
- [29] W.M. Vatavuk, Updating the CE plant cost index, *Chem. Eng.*, 109 (2002) 62–70.
- [30] R.K. Shah, D.P. Sekulic, *Fundamentals of Heat Exchanger Design*, John Wiley & Sons, Hoboken, New Jersey, 2003.
- [31] T.L. Bergman, F.P. Incropera, *Fundamentals of Heat and Mass Transfer*, John Wiley & Sons, 2016.
- [32] B.M. Jacimovic, S.B. Genic, *Thermal Operations and Apparatus, Part 1: Recuperative Heat Exchangers*, Faculty of Mechanical Engineering, Belgrade, 2004.
- [33] S.B. Genić, B.M. Jaćimović, D. Mandić, D. Petrović, Experimental determination of fouling factor on plate heat exchangers in district heating system, *Energy Build.*, 50 (2012) 204–211.
- [34] P. Milanovic, B.M. Jacimovic, S.B. Genic, Experimental measurement of fouling resistance in the heat exchanger of a geothermal heating system, *Geothermics*, 35 (2006) 79–86.
- [35] K.J. Åström, T. Hägglund, *Advanced PID Control*, ISA – The Instrumentation, Systems and Automation Society, Research Triangle Park, NC 27709, 2006.
- [36] G. Zaidner, S. Korotkin, E. Shteimberg, A. Ellenbogen, M. Arad, Y. Cohen, Non Linear PID and Its Application in Process Control, Vol. 26, *Convention of Electrical and Electronics Engineers in Israel (IEEEI)*, IEEE, 2010, pp. 574–577.
- [37] Y.X. Su, D. Sun, B.Y. Duan, Design of an enhanced nonlinear PID controller, *Mechatronics*, 15 (2005) 1005–1024.